American Mineralogist, Volume 91, pages 1815–1830, 2006

Thermodynamics of mixing in pyrope-grossular, $Mg_3Al_2Si_3O_{12}$-$Ca_3Al_2Si_3O_{12}$, solid solution from lattice dynamics calculations and Monte Carlo simulations

VICTOR L. VINOGRAD[1,*] AND MARCEL H.F. SLUITER[2]

[1]University of Frankfurt, Institute of Mineralogy, Senckenberanlage 30, 60054 Frankfurt A.M., Germany
[2]Department of Materials Science and Engineering, Delft University of Technology, 2628CD Delft, Netherlands

ABSTRACT

Static lattice energy calculations (SLEC), based on empirical pair potentials have been performed for a set of 125 different structures with compositions between pyrope and grossular, and with different states of order of the exchangeable Mg and Ca cations. Total energies of a subset of these configurations have been calculated with a density functional electronic structure method (ab initio). The excess energies derived from ab initio and SLEC results agree well with each other. Excess free energies of the 125 structures have been calculated at 300 and 1000 K and at 0 and 3 GPa and cluster expanded in a basis set of 8 pair-interaction parameters. These ordering parameters have been used to constrain Monte Carlo simulations of temperature-dependent properties in the ranges of 300–1500 K and 0–3 GPa. The free energies of mixing have been calculated using the method of thermodynamic integration. The calculations predict the development of a significant short-range and long-range ordering at the intermediate 50/50 composition. The long-range ordered phase with $I4_1$ 22 symmetry becomes stable below 600 K. Two miscibility gaps driven by the stability of the intermediate phase develop at both sides of the 50/50 composition. Activity-composition relations in the range of 600–1500 K and 0–3 GPa are described with high-order Redlich-Kister polynomials.

Keywords: Pyrope-grossular solid solutions, ab initio calculations, atomistic simulations, activity-composition relations

INTRODUCTION

Due to the importance of the activity-composition relations of garnets in petrologic calculations, the pyrope-grossular solid solution, $Mg_3Al_2Si_3O_{12}$-$Ca_3Al_2Si_3O_{12}$, has been extensively studied in recent decades. The availability of calorimetric, volumetric, spectroscopic, and phase equilibrium constraints makes this solid solution a convenient test system for various models of mixing. The calorimetric studies of Newton et al. (1977), Haselton and Westrum (1980), and Dachs and Geiger (2006) have shown that both the enthalpy of mixing and the excess vibrational entropy deviate significantly from the ideal behavior. The enthalpy of mixing reaches about 3 kJ at $x_{pyr} = 0.75$. The excess vibrational entropy is of the order of 1.5 J/(K·mol) at $x_{pyr} = 0.6$ (Haselton and Westrum 1980). Ganguly et al. (1993) and Bosenick and Geiger (1997) have shown that the mixing volumes are positive and asymmetric with a maximal value of about 0.008 J/(bar·mol) at $x_{py} = 0.3$. (All the excess effects are scaled here to one mole of the exchangeable Ca and Mg cations.) There have been many studies that have attempted to derive the mixing properties of garnets directly from phase equilibrium experiments and from compositions of garnets in well-characterized metamorphic rocks (e.g., Berman and Aranovich 1996; Ganguly et al. 1996; Mukhopadhyay et al. 1997). These studies have shown that the phase equilibrium data can be satisfactorily fitted together with the volumetric and calorimetric constraints within the regular solution model. It was clear, however, that these modeling results can be applied only to garnets crystallized at relatively high temperatures or to samples in which Ca-Mg interactions are significantly diluted by the presence of extra components such as Fe^{2+} and Mn^{2+}. Only at these conditions the mixing properties can be approximated with the regular solution model. Bosenick et al. (1995, 1999) have performed ^{29}Si NMR studies on garnets synthesized at high pressures and temperatures and observed that the frequencies of local Ca/Mg configurations deviate from the probabilities of random events. These studies suggested that at lower temperatures the configurational entropy might be significantly decreased from the ideal mixing values due to the development of short-range ordering. To be able to predict the thermodynamic behavior of pyrope-grossular garnets in a wide range of temperatures, several recent studies have attempted atomistic simulations of mixing properties (Dove 2001; Bosenick et al. 2000, 2001a, 2001b; Warren et al. 2001; Vinograd 2001; Vinograd et al. 2004a; Sluiter et al. 2004; Lavrentiev et al. 2006). Although these studies have shown that modern computational tools permit simulation of any observable function of mixing, none of them has been able to demonstrate quantitative agreement with all available experimental constraints. Specifically, none of the studies was able to reproduce the magnitudes of both the enthalpy of mixing and the excess vibrational entropy. No attempts have been made to explain the origin of the observed asymmetry of the functions of mixing. Here we show that a superior model can be developed along the following steps: (1) Development of a transferable set of empirical interatomic potentials. (2) Static lattice energy calculations (SLEC) and lattice dynamics (LD) calculations on a set of structures with

* E-mail: v.vinograd@kristall.uni-frankfurt.de

randomly varied cation configurations. (3) Ab initio calculations on a selected set of configurations used for the SLEC. (4) Comparing the excess energies derived from the SLEC and ab initio calculations and modifying the empirical potentials in the case of a poor agreement. (5) Cluster expanding the excess free energies of the simulated structures. In this procedure a property is decomposed in terms of contributions from small figures or clusters. (6) Using the cluster expansion model to obtain temperature-dependent properties by Monte Carlo simulation. (7) Calculation of the free energies of mixing and ordering by thermodynamic integration of the Monte Carlo results. (8) Refitting the free energies of mixing to simple polynomial equations useful for phase equilibrium calculations.

Simulation procedure

The empirical potentials

Our set of potentials involves two-parameter Metal-Oxygen (M-O) Buckingham potentials, three-body O-M-O angle-bending terms and the shell model for the oxygen polarizability as described by Sanders et al. (1984). The studies of Winkler et al. (1991), Patel et al. (1991), and Sainz-Diaz et al. (2001) have shown that the potentials of this type together with the assumption of formal charges on cations and anions permit a good description of structure and elasticity data of many silicates and aluminosilicates. However, low quality fits are usually observed for dense structures, such as stishovite and corundum. Vinograd et al. (2004b) have noted that in the dense structures it is especially difficult to fit the short cation-cation distances. Following Vinograd et al. (2004b, 2006a) we have multiplied formal cation and anion charges by the common factor 0.85, so that the charges of Mg and Ca, Al, Si, and O have been reduced to the values of 1.7, 2.55, 3.4, and –1.7, respectively. Such a reduction leads to a much better transferability of the potentials within oxide structures of variable density. The possible reason for this improvement is that the formal charges on cations cause too strong a cation-cation repulsion. The reduction of the charges by a small common factor removes this problem, but conveniently preserves the charge balance. The potentials have been developed using the relax-fitting procedure (Gale 1996) as implemented in the GULP program (Gale 1997) by fitting to structural parameters and elastic stiffness coefficients of a large set of minerals. The potentials of the Mg-Al-Si-O system have been described previously by Vinograd et al. (2006a). Here, we have extended the potentials to the Ca-Mg-Al-Si-O system. Two Ca-O potentials have been developed. The first potential has been derived by fitting to structure and elasticity data of a large set of Ca-bearing minerals including lime, larnite, Ca-Tschermak pyroxene, diopside grossular, gehlenite, and anorthite. This potential is labeled in Table 1 as $Ca^{[6-8]}$-O to emphasize its transferability within minerals with different Ca coordination by oxygen. It was observed, however, that this potential predicts the excess enthalpy of the pyrope-grossular solid solution that is about 30% too large to be consistent with the calorimetric data of Newton et al. (1977) and with our ab initio calculations (see the following section). We then excluded lime, larnite and the pyroxenes from the fit and obtained a new potential, which gave an improved description of the structure and elasticity data of grossular, anorthite, and gehlenite. The elastic constants of grossular and anorthite have been adopted from the compilation of Bass (1995). The structural parameters of anorthite and grossular have been taken from Angel et al. (1990) (sample from Somma) and Rodehorst et al. (2002) (synthetic sample, T = 156 K), respectively. The structural parameters of gehlenite were taken from Swainson et al. (1992). This potential is labeled as $Ca^{[8]}$-O in Table 1 to emphasize its special applicability to the structures in which Ca occurs in higher coordination. This potential shows a much better agreement with our ab initio calculations and is used here for the SLEC calculations of a large set of structures with composition between pyrope and grossular. Our experience suggests (Vinograd et al. 2004a) that the ability of a model to predict the correct magnitude of the mixing enthalpy depends primarily on the adequate description of the elasticity and structure data. Therefore, in Tables 2 and 3 we compare the predicted structural parameters and elastic stiffness coefficients of pyrope and grossular with the available experimental data. Table 4 lists the predicted infrared frequencies in pyrope and grossular together with the experimental data of Boffa Ballaran et al. (1999). The predicted frequencies of low-energy modes are in excellent agreement with experiment, while the three high-energy modes on average are lower than the experimental values by about 10%. This discrepancy should have only a minor influence on the calculated excess properties of garnets since the high-energy modes reflect atomic motions within SiO_4 tetrahedra, which play a passive role in the mixing process. Bosenick et al. (1996), Kolesov and Geiger (1998), and Dachs and Geiger (2006) suggested that the excess entropy of mixing arises from softening of the low-energy modes at the intermediate compositions. As we will show below, the magnitude of the excess vibrational entropy depends

Table 1. The empirical interatomic potentials used in the present study with the notation [4], [6], and [8] referring to the coordination number of the associated species

Buckingham

Interaction	A (eV)	ρ (Å)	C (eV Å^6)
Al[4-6](core)-O(shell)	1262.2081	0.286370	0.0
Mg[6-8](core)-O(shell)	1432.8544	0.277265	0.0
Ca[8](core)-O(shell)	3285.2403	0.271592	0.0
Ca[6-8](core)-O(shell)	2707.5868	0.282660	0.0
Si[4-6](core)-O(shell)	1073.4668	0.298398	0.0
O(shell)-O(shell)	598.8996	0.314947	26.89746

Spring

Interaction	K (eV/Å^2)
O(core)-O(shell)	56.5598

Three-body

Interaction	k_θ (eV/rad^2)	θ (degree)
O(shell)-Si[4]-O(shell)	0.77664	109.47
O(shell)-Si[6]-O(shell)	2.2955	90.0
O(shell)-Al[4]-O(shell)	1.2883	109.47
O(shell)-Al[6]-O(shell)	1.8807	90.0

Notes: The charges on the oxygen core and shell are 0.746527 and –2.446527, respectively. Cutoff distance for the Buckingham potentials is 12 Å.

Table 2. Structural parameters of pyrope and grossular as calculated with the SLEC and DFT GGA in comparison with experimental data

Grossular

Parameter		XRD	SLEC	DFT-GGA
a (Å)		11.840*; 11.837†	11.8215	11.9668
Volume (Å^3)		1659.80*; 1658.53†	1652.013	1713.698
O 96h	x	0.0381*; 0.0382†	0.0372	0.0383
	y	0.0456*; 0.0454†	0.0464	0.0452
	z	0.6514*; 0.6513†	0.6510	0.6517

Pyrope

Parameter		XRD	SLEC	DFT-GGA
a (Å)		11.439; 11.455§	11.446	11.5658
Volume (Å^3)		1496.80‡; 1502.89§	1499.418	1547.132
O 96h	x	0.0330‡; 0.0332§	0.0319	0.0329
	y	0.0503‡; 0.0497§	0.0514	0.0503
	z	0.6533‡; 0.6537§	0.6532	0.6538

* Rodehorst et al. 2002.
† Geiger and Armbruster 1997.
‡ Pavese et al. 1995.
§ Zhang et al. 1998.

Table 3. Elastic stiffness coefficients for pyrope and grossular as calculated with the SLEC in comparison with experimental data

Grossular

Stiffness coefficient	Observed (GPa)	SLEC (GPa)
C_{11}	321.7*; 318.8†	323.8
C_{44}	104.6*; 102.9†	100.53
C_{12}	91.4*; 92.1†	102.12
Bulk modulus	168.4*; 167.8†; 175‖	176.03

Pyrope

Stiffness coefficient	Observed (GPa)	SLEC (GPa)
C_{11}	296.2‡; 295.8§	316.04
C_{44}	91.6‡; 90.8§	104.62
C_{12}	111.1‡; 117.8§	108.59
Bulk modulus	172.8‡; 177.0§; 171‖	177.74

* Bass 1989.
† Isaak et al. 1992.
‡ O'Neill et al. 1991.
§ Leitner et al. 1980.
‖ Zhang et al. 1999.

on the relative change of the vibrational frequencies of the end-members due to the extension and contraction of their structures as they adjust to the common volume at an intermediate composition of the solid solution. In this respect it is important that the potentials correctly predicted the differences in the vibrational frequencies of the end-members and their changes as function of volume. The present set predicts consistently larger frequencies of pyrope relative to those of grossular. A further test of the accuracy of the potentials is given in the next section.

Quantum mechanical calculations

While calculations based on empirical potentials are computationally very efficient, the predictive power of this approach requires an independent test. It is important that the potentials are able to predict correct energy differences between structures with different arrangements of the exchangeable cations. Here we compare SLEC results for a selected set of structures with parameter-free quantum mechanical calculations based on the density functional theory (DFT) (Hohenberg and Kohn 1964; Kohn and Sham 1965; Parr and Yang 1989; Jones and Gunnarsson 1989). We used the generalized gradient approximation (GGA), in the form suggested by Perdew et al. (1996). To avoid explicit description of tightly bound core electrons, the approach employs "ultrasoft" pseudopotentials (Vanderbilt 1990; Kresse and Hafner 1994). In the present study we have used the VASP code (Kresse and Furthmüller 1996). The cut-off energy for the plane wave expansion was 400 eV. Calculations were performed for a unit cell consisting of 160 atoms (24 exchangeable cations) and integrations in reciprocal space utilized the Γ-point only. In all calculations, all symmetry independent structural parameters were varied simultaneously in the search for the ground state geometry. The parameters of the "relaxed" (optimized) structures of pyrope and grossular are given in Table 2, where they are compared to experimental values and to the results of the calculations based on empirical potentials. We also computed several structures with mixed Ca-Mg distributions. The composition of these structures and their excess energies relative to the mechanical mixture of pyrope and grossular are given in Table 5. Sluiter et al. (2004) reported the excess energies of some of these structures previously. The majority of these structures were constructed from pure grossular and pyrope by substituting one or two atoms with atoms of the other sort. The structures with two Ca atoms in the pyrope matrix and with two Mg atoms in the grossular matrix differ in relative positions of the impurities. The structures numbered 1, 2, 3, and 4 correspond to the location of the impurity pair at the first, second, third, and fourth nearest-neighbor distances, respectively. The notations 4a and 4b are used to distinguish two symmetrically different structures. In fact, there are two symmetrically different pairs of the fourth-nearest neighbors: the pair 4b contains an Al atom exactly in the middle of the two dodecahedral sites, while the 4a vector does not cross any other atom (Fig. 1). (The existence of the two types of pairs of the fourth-nearest neighbors was missed in all previous studies. Here we show that distinguishing these pairs has an important implication for the predicted ground state structure.) We have also calculated the ab initio total energy of an ordered structure with the 50/50 composition. This structure with $I4_122$ symmetry has been manually constructed by maximizing numbers of dissimilar (Ca-Mg) contacts at the third and the fourth "b" distances (Figs. 1a and 1b). The ab initio calculations have confirmed that this structure has the lowest total energy among the tested mixed configurations. Table 5 shows that the results of the empirical and ab initio calculations are in good agreement with each other. This permits us to apply the computationally efficient SLEC approach to several other structures.

The SLEC and lattice dynamics calculations

The fully relaxed SLEC calculations have been performed with GULP in the 160-atom primitive unit cell on a set of randomly modified structures (configurations) with $x = 0$ (1), $x = 0.04167$ (1), $x = 0.0833$ (8) $x = 0.25$ (25), $x = 0.5$ (50), $x = 0.75$ (25), $x = 0.9167$ (8), $x = 0.95833$ (1), and $x = 1$ (1) compositions. Here x denotes the mole fraction of pyrope. The numbers of the sampled structures with the same composition are given in parentheses. We have also performed the SLEC for 4 configurations with $x = 0.5$ composition, which have been produced by manual disordering of the $I4_122$ structure. The $I4_122$ structure has the lowest static energy at the 50/50 composition. Subsequently, this result was confirmed by Monte Carlo simulations (see below). Results from the first set of calculations, at zero K and zero pressure, are displayed in Figure 2 where the excess static energies are plotted. Some of these energies also appear in Table 5. The other sets of calculations were performed at 300 and 1000 K and at 0 and 3 GPa with the ZSISA (Zero Static Internal Stress Approximation, Allan et al. 1996) as implemented

TABLE 4. The comparison between the observed and predicted frequencies of infrared-active modes

Peak	Grossular		Pyrope	
	Observed	Predicted	Observed	Predicted
R	155	148		149
Q	180	176	150	158
P	205	199		195
N	240	223	210	218
O	300	284	260	253
M	355	354		314
L		371	350	353
K	400	395	390	376
J		419	420	410
I	455	441	465	444
H	475	450	490	468
G	520	467	540	516
F	540	518	580	564
E	615	578		622
D	840	767	875	788
C	860	789	910	812
B	910	858	980	899

Notes: Values are in cm^{-1}. The experimental data and the nomenclature of the IR bands are from Boffa Ballaran et al. (1999).

TABLE 5. The comparison between empirically and ab-initio calculated excess lattice energies of selected configurations

Structure	Empirical potentials	Ab initio
$Ca_{23}Mg_1$	0.5117	0.5096
$Ca_{22}Mg_2$ (1)	0.9322	1.0042
$Ca_{22}Mg_2$ (2)	0.9200	0.9142
$Ca_{22}Mg_2$ (3)	1.6123	1.6834
$Ca_{22}Mg_2$ (4a)	0.8403	0.9355
$Ca_{22}Mg_2$ (4b)	0.9992	1.0765
Ca_2Mg_{22} (1)	1.0610	1.1990
Ca_2Mg_{22} (2)	1.0787	1.1656
Ca_2Mg_{22} (3)	1.7346	1.8188
Ca_2Mg_{22} (4a)	1.0356	1.1781
Ca_2Mg_{22} (4b)	1.2047	1.4275
Ca_1Mg_{23}	0.5886	0.6640
$Ca_{12}Mg_{12}$ ($I4_122$)	0.1361	0.0579

Notes: Values are in kJ/mol of exchangeable atoms. All values are scaled to the mixture of pyrope and grossular in equivalent fractions.

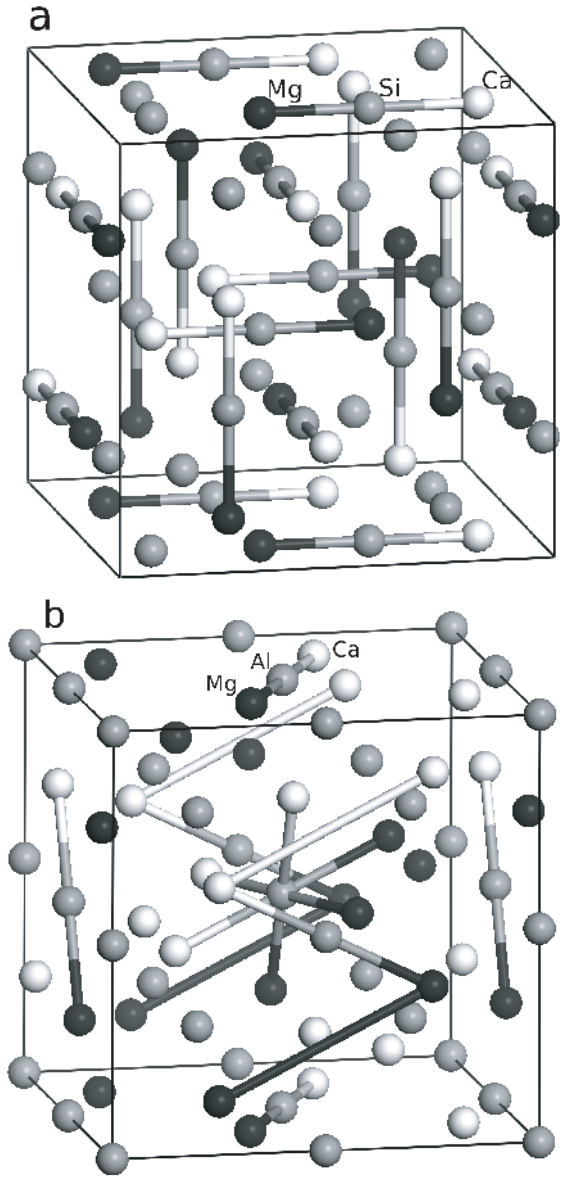

FIGURE 1. Arrangement of cations in the ordered garnet with the $I4_122$ symmetry. The sticks show the interactions between the third (**a**) and fourth (**b**) neighbors. White and black spheres correspond to Mg and Ca atoms, respectively. The gray spheres denote either Si (**a**) or Al (**b**). The 4b interactions can be distinguished from the 4a interactions by the presence of an Al atom exactly at the mid-point between the neighboring dodecahedral sites.

in GULP. In these calculations the Gibbs free energy (see a comment below) is minimized. The Gibbs free energy includes the static energy, the vibrational free energy and the *PV* term. The ZSISA was preferred over the conventional free energy minimization because it is more stable at high temperatures. The problem is that in the conventional free energy minimization the frequencies are calculated at a point where the forces are not zero (the frequencies are obtained from the second derivatives of the internal energy, while the fractional coordinates and unit-cell parameters correspond to the free energy minimum).

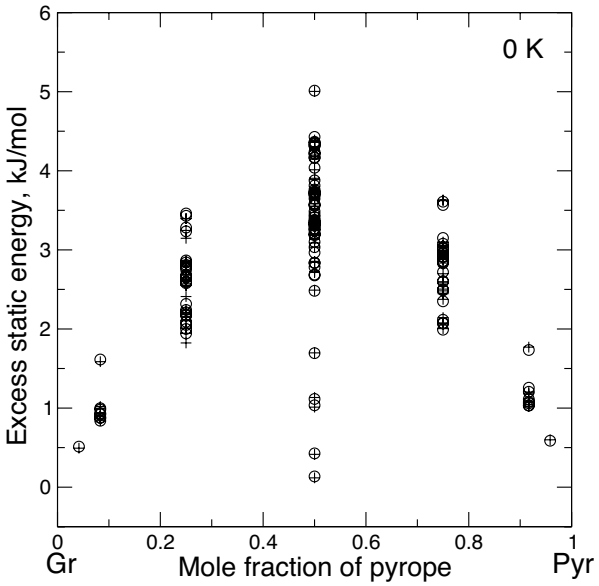

FIGURE 2. The excess static lattice energies of the studied structures. (The energies are scaled relative to the weighted sum of the energies of grossular and pyrope.) Circles are the GULP results, the crosses are the results of the cluster expansion.

Therefore the harmonic approximation is violated. In ZSISA the internal degrees of freedom are minimized with respect to the internal energy, which guarantees zero force at the point of the frequency calculation. Therefore, ZSISA is consistent with the quasi-harmonic approximation; however, the calculated property is not exactly the Gibbs free energy, because only the external degrees of freedom are minimized with respect to the pressure and temperature dependent terms. Figures 3a and 3b show the excess Gibbs free energies of the sampled configurations at 300 and 1000 K, respectively. Figures 4a, 4b, 5a, and 5b show the excess volumes and the excess vibrational entropies, respectively, calculated at zero pressure. The increase in pressure up to 3 GPa leads only to a slight increase in the excess free energies, which amounts to about 0.5 kJ/mol at 1000 K at the intermediate composition.

The SLEC and lattice dynamics calculations show that the type and degree of asymmetry in the excess mixing properties with respect to 50/50 composition is strongly dependent on the property under consideration. The maximum of the excess static energy is shifted in the direction of the smaller component, while the maximum of the excess vibrational entropy is displaced in the direction of the larger component. It is also evident that there is a strong positive correlation between the excess volumes and entropies, which we believe to be responsible for the similarity in the asymmetry of these properties. This correlation is illustrated in Figure 6.

Virtual crystal calculations

The predicted asymmetry of the mixing functions can be well understood within the virtual crystal approximation. Following Ferreira et al. (1988) we assume that the actual mixing process can be split into two stages: (1) the volume deformation (the lattices of

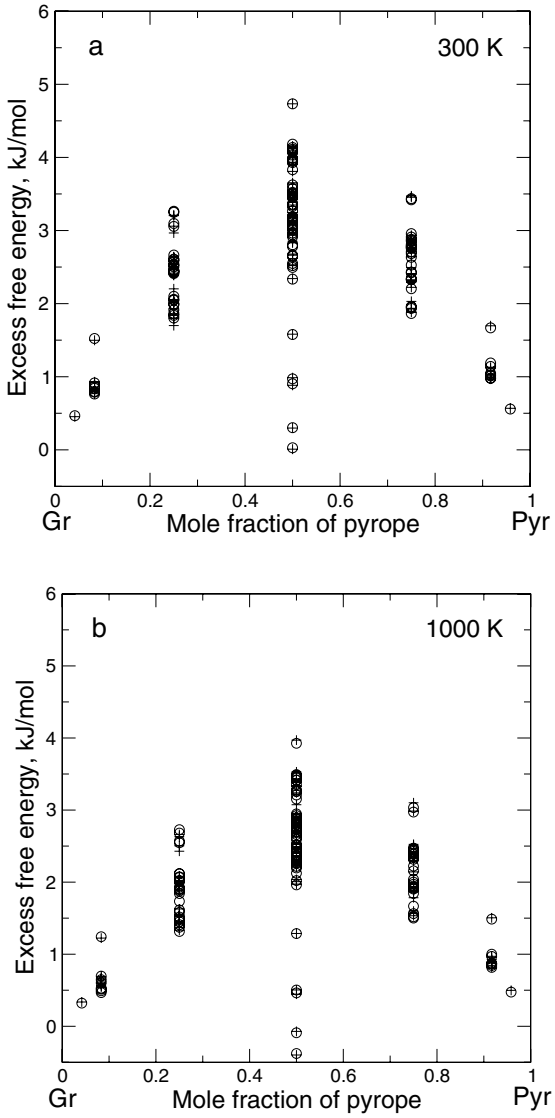

FIGURE 3. The excess Gibbs free energy calculated with ZSISA (zero static internal stress approximation) at 300 K (**a**) and 1000 K (**b**). Symbols are the same as in Figure 1. The excess quantity is defined relative to the weighted sum of the Gibbs free energies of grossular and pyrope.

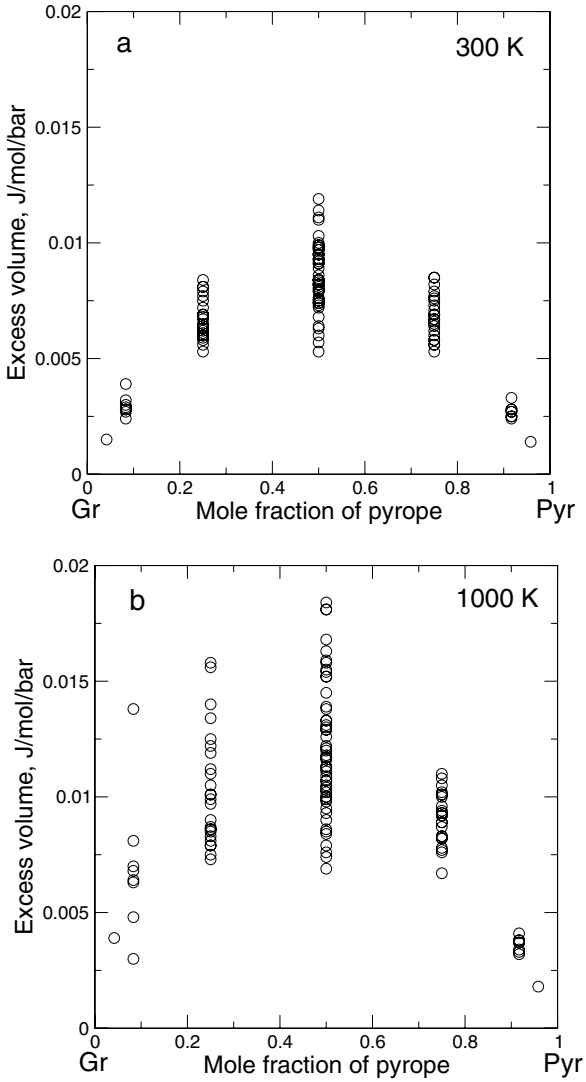

FIGURE 4. The excess volume calculated with ZSISA at 300 K (**a**) and 1000 K (**b**).

the end-members are homogeneously deformed, i.e. expanded or contracted, until their cell dimensions and volumes equalize) and (2) the actual mixing via cation diffusion on the already deformed lattice with the subsequent local relaxation of the structure. The virtual crystal calculations are concerned with the energetic and entropic effects that occur at the first stage. We assume for simplicity that the volume changes linearly with the composition of the mixture. This permits us to calculate the increase in the static energy of pyrope, ΔE_1, when its volume is linearly expanded to the volume of grossular, and the increase in the static energy of grossular, ΔE_2, when its volume is linearly contracted to the volume of pyrope. The results of these calculations together with the total effect are plotted in Figure 7. The total volume deformation energy is calculated with the equation:

$$E_{VD} = x_1\Delta E_1 + x_2\Delta E_2 \quad (1)$$

where x_1 and x_2 are mole fractions of grossular and pyrope, respectively. Since the contraction of grossular requires more energy than the expansion of pyrope, the maximum of the total energy is shifted in the direction of pyrope. Calorimetric data of Newton et al. (1977) exhibit a similar asymmetry with the maximum shifted in the direction of pyrope. The magnitude of the volume deformation energy greatly exceeds the measured calorimetric effect, however. This, as we will confirm later, suggests that the energy effect of the second mixing stage is negative. Similar calculations reveal the origin of the asymmetry of the excess entropy. We have calculated the increase in the vibrational entropy of pyrope at 300 K when its volume is linearly expanded to the volume of grossular and the decrease in the entropy of grossular, when its volume is contracted to the

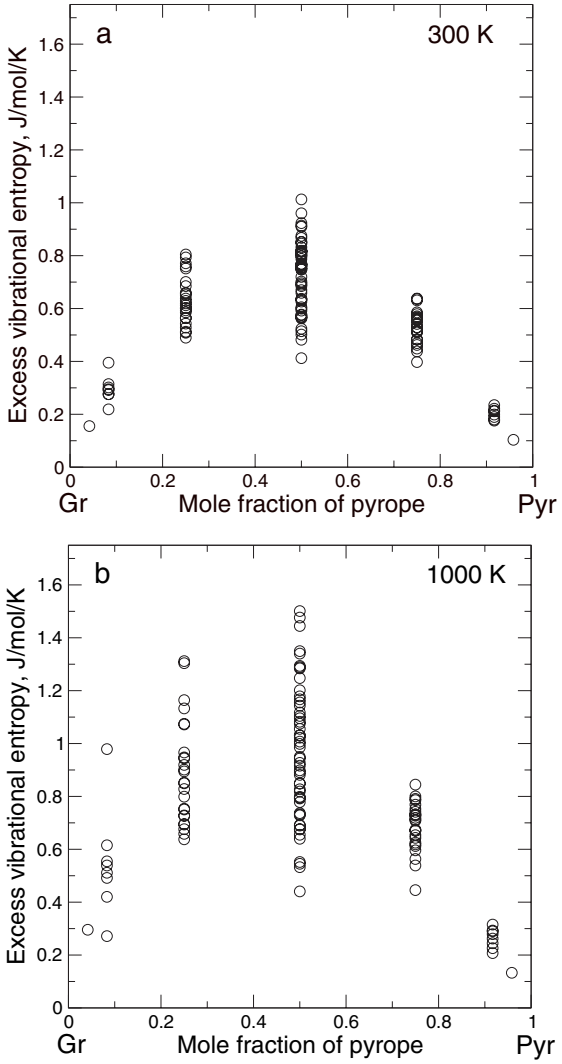

FIGURE 5. The excess vibrational entropy calculated with ZSISA at 300 K (**a**) and 1000 K (**b**). The excess quantity is defined with respect to the weighted sum of the vibrational entropies of grossular and pyrope at the given temperature.

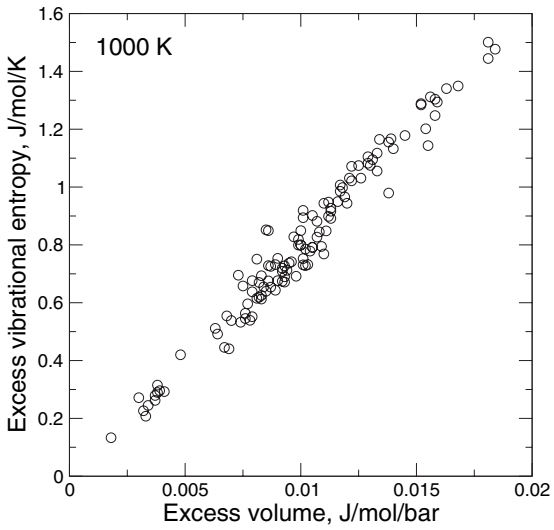

FIGURE 6. Correlation between the excess vibrational entropy and the excess volume at 1000 K and zero pressure.

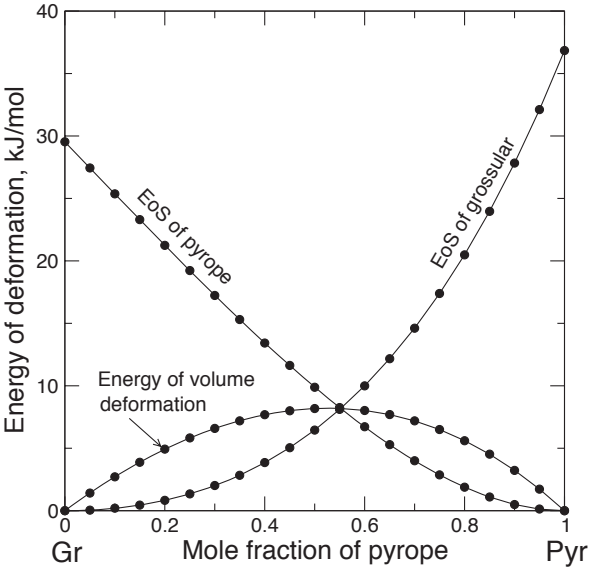

FIGURE 7. The equations of state (energy vs. volume) of pyrope and grossular and the total volume deformation energy plotted vs. the mole fraction of pyrope. It is assumed that volume changes linearly vs. the composition.

standard volume of pyrope. Since the increase in the entropy of pyrope exceeds the decrease of the entropy of grossular, the total change in the vibrational entropy of the mixture is positive with the maximum shifted prominently in the direction of the end-member with the largest volume (Fig. 8). The above variation in the vibrational entropy of pyrope and grossular can be rationalized if one considers the change in the force constants associated with the vibrations of Mg and Ca in the dodecahedral cages. Sluiter et al. (2004, Table II) using the DFT GGA have calculated the differences of the force constants of Mg and Ca in the two contrasting cases. The first case corresponds to the vibration of an atom in the cell of the end-member composition ($Mg_{24}Al_{16}Si_{24}O_{96}$ or $Ca_{24}Al_{16}Si_{24}O_{96}$), the second case corresponds to the situation when Mg or Ca is an impurity ($MgCa_{23}Al_{16}Si_{24}O_{96}$ or $CaMg_{23}Al_{16}Si_{24}O_{96}$). These calculations have shown that the force constants of Mg in the impurity state are smaller than those in the end-member state, while the force constants of Ca are larger in the impurity state. These effects are well understood considering that the size of the polyhedron centered on Mg increases in the impurity case, while the size of the polyhedron centered on Ca decreases in the impurity state. The nontrivial observation is that the decrease in the force constants of Mg is greater than the increase in the force constants of Ca. This is consistent with the much stronger increase in the entropy of pyrope on extension. An additional factor is that the relative volume change of pyrope, $\Delta V/V_{Pyr} = 0.102$, is larger than that of grossular, $\Delta V/V_{Gr} = 0.093$. The positive correlation between the excess volumes and the excess entropies (Fig. 6) explains the experimentally observed asymmetry of the excess volume. The correlation has the same

origin as the thermal expansion. An increase in volume leads to a decrease in vibrational frequencies and consequently to an increase in the vibrational entropy. Due to the positive excess entropy, the increase in volume becomes particularly advantageous at intermediate compositions, where the TS_{excess} term is larger. For the same reason the excess volume becomes larger at high temperatures. The higher excess volume at higher temperature causes a further increase in the excess entropy.

The above analysis suggests that a significant part of the mixing energy, the excess entropy and the excess volume have a non-configurational origin. In fact, the calculated volume deformation energy and the excess entropy are the properties of the mixture of pyrope and grossular deformed to a common volume. Obviously, any property that relates to the mixture of the end-members does not depend on the arrangement of atoms within the solid solution. (Here we avoid saying "a mechanical mixture" because this term usually is applied to mixtures with properties that vary linearly with the composition. The more appropriate term is "a strained mixture.")

Cluster expansion of the SLEC results

The aim of the cluster expansion is to find a simple equation, which fits the energies of all simulated configurations and, hopefully, predicts the energy of any other possible configuration. One popular form for such an expansion is known as the *J* values formalism (e.g., Dove 2001; Vinograd 2001 and references therein)

$$E_i \approx 1/2 \sum_n z^{(n)} P_{AB^{(n)}} J_n + E_0 \quad (2)$$

where $z^{(n)}$, $P_{AB^{(n)}}$, and J_n are the coordination numbers, fractions of AB-type pairs and effective cluster interactions for pairs of the order n. J_n corresponds to the energy of the exchange reaction AA + BB = 2AB between atoms A (Mg) and B (Ca) located at the n-th distance. When this equation is applied to the excess energies, E_0 absorbs the non-configurational effects, while the sum of the J values describes all effects of relaxation due to the formation of the solid solution. The main effect of the solid solution formation is the production of AB pairs from AA and BB pairs. When the energy of the strained mechanical mixture is separated out as the E_0 term, the J values permit clear physical interpretation: These are the energies that are released when AA and BB pairs, forced to match the average interatomic distance at a composition x, are allowed to exchange atoms and make pairs of AB and BA types matching the same interatomic distance. The energy is released (usually) as it is easier to match the interatomic distance at an intermediate composition with two atoms of different size as opposed to the same atoms. The pairs of the same atoms will be either too large or too small with respect to the average distance. Since the energy of the strained mechanical mixture can be well approximated with a two-parameter polynomial (e.g., Vinograd et al. 2004a), it is convenient to expand the E_0 term as follows:

$$E_0 = x_1 x_2 (x_1 A_{12} + x_2 A_{21}) \quad (3)$$

To determine the set of the J values for each of the 125 structures, we have calculated the fractions (frequencies of occurrence) of pairs of dissimilar atoms at 7 distances, as specified in Table 6. Since there are two symmetrically different pairs at the 4th distance, each configuration i is characterized by 8 frequencies, P_n [the factor $1/2z^{(n)}$ is included in the frequency value], and by a value of the relaxed excess energy E_i, where the excess value is defined relative to the weighted sum of the relaxed energies of pyrope and grossular. The whole set of configurations is thus characterized by the 125 × 8 frequency matrix **P** and with the 125-element vector **E**. With each dissimilar pair we associate a constant J_n. The 8-element vector **J** is traditionally found by solving the matrix equation $\mathbf{J}=\mathbf{P}^{-1}\mathbf{E}$ using a least squares method. Since E_0 is a configuration-independent term, its value must not be mapped onto the J values expansion. Therefore, the **J** vector is found from $\mathbf{J}=\mathbf{P}^{-1}\mathbf{E}'$, where the vector **E**' is obtained from the vector **E** by subtracting the value of E_0 from each element. We calculate also the vector **E**', which represents the approximation to **E**' predicted with the J values expansion. Finally, we search for the values of A_{12} and A_{21}, which result in the best fit. Because of

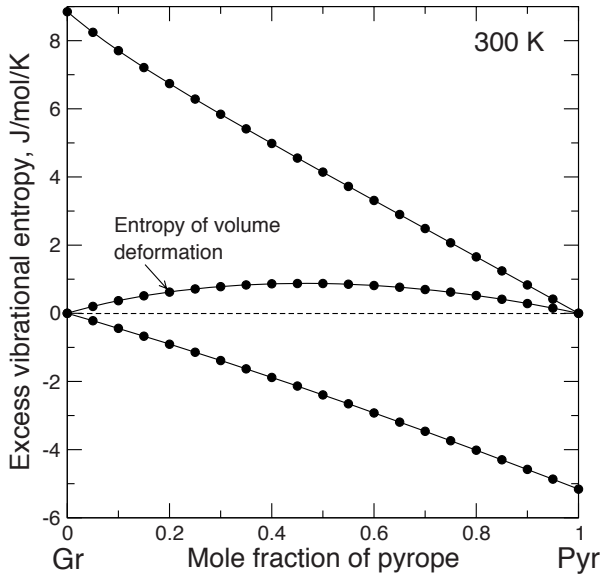

FIGURE 8. The entropic equations of state (entropy vs. volume) of pyrope and grossular and the total excess entropy plotted vs. the mole fraction of pyrope. The vibrational entropy is calculated at 300 K. It is assumed that volume changes linearly with composition.

TABLE 6. The final parameters of the fitted cluster expansion.

		Pairwise energies				
n	Distance (Å)	0 K 0 GPa	300 K 0 GPa	1000 K 0 GPa	300 K 3 GPa	1000 K 3 GPa
1	3.051	−0.4270	−0.6810	−1.4659	−0.4325	−1.0432
2	5.355	−0.4229	−0.5294	−0.7916	−0.3580	−0.5978
3	5.725	−8.4223	−8.2859	−7.7208	−8.2204	−7.9874
4a	6.400	0.5213	0.4722	0.4386	0.5002	0.4170
4b	6.400	−1.6159	−1.4713	−1.1275	−1.6680	−1.3334
5	6.713	−2.9661	−2.8426	−2.4448	−2.8149	−2.5370
6	7.840	0.1377	0.0875	−0.1034	0.0944	−0.0310
7	8.096	−0.0192	−0.0091	0.0494	0.0182	0.0132

		The elastic term			
Parameter	0 K	300 K 0 GPa	1000 K 0 GPa	300 K 3 GPa	1000 K 3 GPa
A_{12}	33.429	33.602	34.485	33.608	34.300
A_{21}	30.541	30.478	30.075	30.372	30.200

Note: The values are in kJ per mole of dodecahedral cations.

a strong correlation between the J_n and A_{ij} parameters, we have introduced an additional constraint in the fit requiring A_{12} and A_{21} parameters to stay within the interval of 25–45 kJ/mol. Values of this order of magnitude would match the volume deformation energy (Fig. 7). The results of the fit are shown in Table 6.

The J values calculated in the way described above exclude the effect of the vibrational entropy. To include the effect of vibrations, we directly expanded the excess Gibbs free energies. The only difference between the expansion of the static energy and the expansion of the Gibbs energy, φ, is that the E_i values in Equation 2 are replaced with φ_i and the E_0 value is replaced with φ_0, where φ_0 includes both the volume deformation and the excess vibrational free energy of the strained mechanical mixture. It is assumed that φ_0 can be approximated with the same equation as the E_0. The results of these calculations are displayed in Table 6. The same analysis has been applied to the excess Gibbs free energies, which correspond to the calculations at nonzero pressure. The J values then absorb both the $-TS_{vib}$ and PV_{ex} terms. These J values are also listed in Table 6. Figure 9 illustrates the accuracy of the cluster expansion of the Gibbs free energy calculated at 1000 K. An even better accuracy is observed in the cluster expansion results corresponding to the 0 and 300 K sets. Evidently, the high accuracy of the cluster expansion makes it feasible to efficiently simulate a Boltzmann probability distribution of the dodecahedrally coordinated Mg/Ca atoms with the Monte Carlo method.

Monte Carlo simulations

Monte Carlo simulations have been performed using a $4 \times 4 \times 4$ supercell with periodic boundary conditions (1536 dodecahedral sites) with our own code. The swapping of sites has been performed according to the Metropolis algorithm (Metropolis et al. 1953). The energy differences between the subsequent steps have been calculated using Equation 2. The temperature dependent properties have been calculated on a grid of 25 different compositions across the pyrope-grossular binary in the interval of 300–1500 K with a step of 100 K. Each point in *T-X* space was equilibrated for 500 000 Monte Carlo steps and additional 500 000 steps were used for the calculation of the averages. The first set of calculations employed temperature independent (T-I) J values, reflecting the effect of the static lattice energy only. The second set employed temperature dependent (T-D) J values, which incorporated the effect of the excess vibrational energy. These J values have been linearly interpolated between the values corresponding to 300 and 1000 K and linearly extrapolated to 1500 K. The averaging over the Monte Carlo results constrained with the temperature independent J values gives the isotherms of the excess static lattice energy. These isotherms are compared with the experimentally measured enthalpies in Figure 10. The high-temperature isotherms are in reasonable agreement with the calorimetric measurements of Newton et al. (1977), which have been performed on samples with a relatively disordered cation distribution. (The samples were synthesized at 1400 °C and 30 kbar.) Figure 11 shows the isotherms of the excess Gibbs free energy, which have been calculated from the Monte Carlo simulations constrained with the T-D J values. These values are consistently smaller than the excess enthalpies due to the vibrational free energy. Note that the excess Gibbs free energy is defined here with respect to the mechanical mixture of the end-members, but not with respect to the free energy of mixing of an ideal solid solution. The configurational entropy is not yet included in the Gibbs free energy values. At temperatures below 600 K both the excess enthalpy and the excess Gibbs free energy significantly decrease at the intermediate composition. The region where the isotherms decrease rapidly corresponds to the development of LRO associated with the cubic/tetragonal, $Ia\bar{3}d/I4_122$ transition. The LRO parameter variation across the transition was investigated in special Monte Carlo runs both with

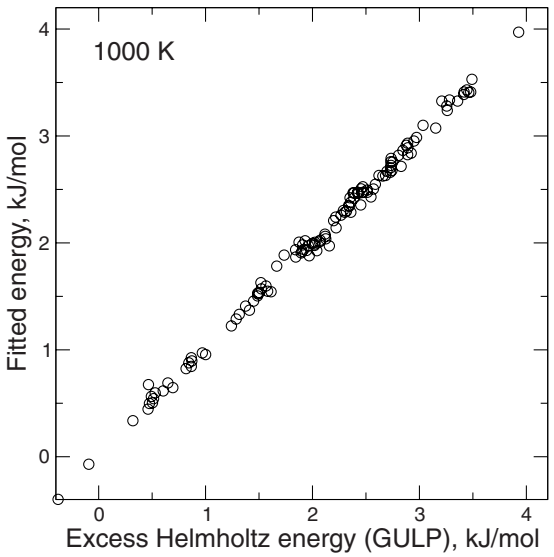

FIGURE 9. Correlation between the cluster expanded and the original (GULP) values of the excess Gibbs free energies of the 125 structures at 1000 K and zero pressure.

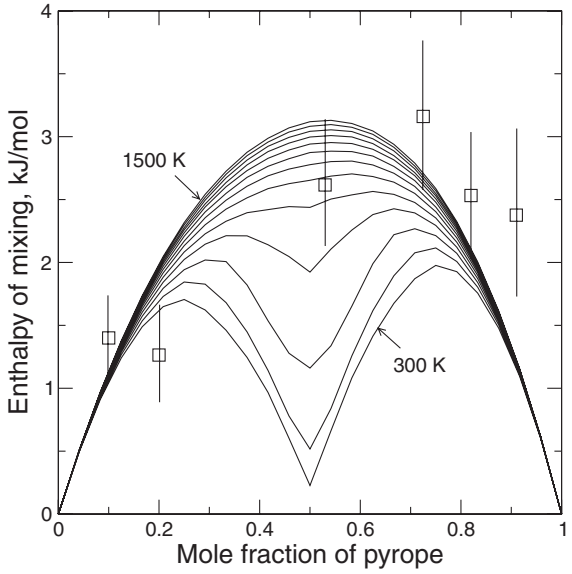

FIGURE 10. The enthalpy of mixing calculated from the Monte Carlo simulations performed with the temperature independent J values. The squares show the experimental data of Newton et al. (1977).

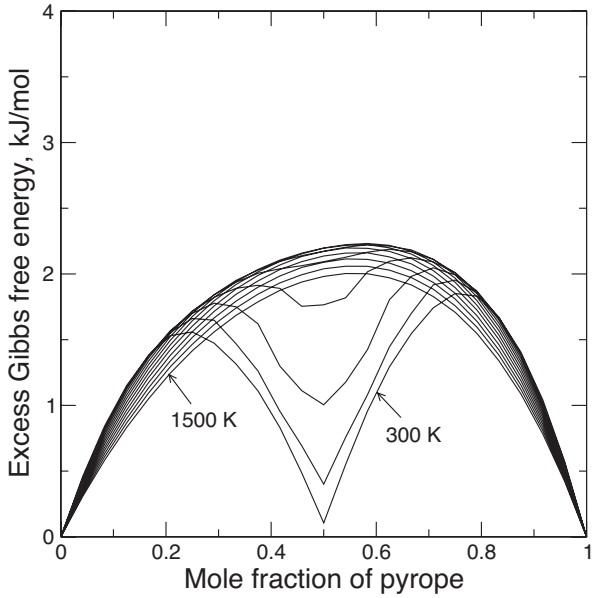

FIGURE 11. The excess Gibbs free energy of mixing calculated from the Monte Carlo simulations performed with the temperature dependent *J* values.

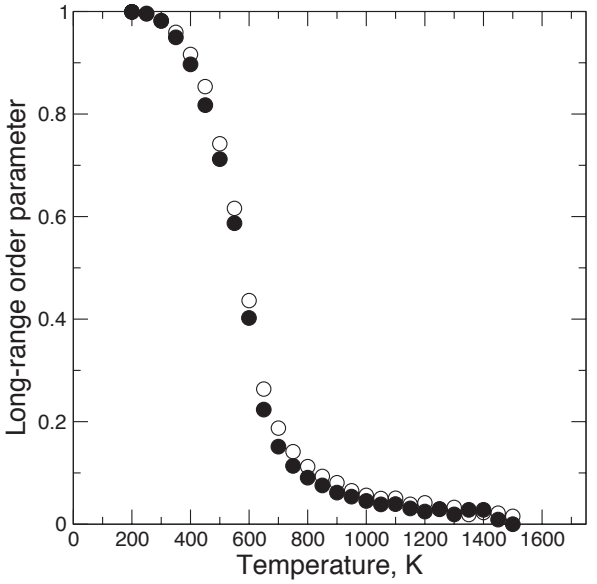

FIGURE 12. The temperature dependence of the long-range order parameter as calculated from Monte Carlo simulations at zero pressure. Open and filled circles correspond to the calculations performed with the temperature-independent and temperature-dependent *J* values, respectively.

the T-I and T-D *J* values at the 50/50 composition (Fig. 12). The LRO parameter has been defined as follows

$$Q_{od} = \frac{P_{A\alpha} - P_{A\beta}}{P_{A\alpha} + P_{A\beta}} \quad (4)$$

where $P_{A\alpha}$ and $P_{A\beta}$ are the probabilities of finding an A atom (e.g., Mg) in two dissimilar dodecahedral sites. These two sites become structurally distinct in the tetragonal phase. However, these probabilities (frequencies) cannot be directly determined from the site occupancies derived from the Monte Carlo simulations because the LRO fluctuates between the three equally probable orientations. Therefore, we have calculated the LRO parameter indirectly from the probabilities of AA pairs. The pair probabilities are much less affected by the spontaneous changes in the LRO orientation. Statistical theories of LRO (e.g., Vinograd and Putnis 1999) suggest that at short distances the pair probabilities are functions of both short-range order (SRO) and LRO parameters. However, the SRO correlations rapidly vanish with distance and by measuring the AA probability at the maximum separation in the Monte Carlo supercell one can be fairly sure that the SRO contribution is insignificant. (This distance was equal to 22.89 Å in our simulations.)

Using Equation 4, the fractional occupancies of the sites can be written as functions of the LRO parameter. Therefore

$$P_{A\alpha A\beta} = P_{A\alpha}P_{A\beta} = P_A^2(1 + Q_{od})(1 - Q_{od}) = (1 - Q_{od}^2)/4 \quad (5)$$

where P_A is the probability of finding an A atom in the whole lattice ($P_A = 1/2$ at the intermediate composition). From Equation 5 one can easily recalculate Q_{od} (Fig. 12). It is clear that the SRO/LRO transition occurs in pyrope-grossular garnets at about 600 K. The nonzero values of the LRO parameter at the higher temperatures are due to the relatively small size of the simulation cell. Including the effect of vibrations has only a minor effect on the temperature of the onset of the LRO. The predicted LRO in the pyrope-grossular garnets disagrees with the earlier result of Bosenick et al. (2000) and Vinograd et al. (2004) who observed at the 50/50 composition the development of short-range order only. This new result is due to the different treatment of the ordering interactions between the fourth-nearest neighbors. In the previous studies J_{4a} and J_{4b} have been treated as the same J_4 interaction. We show here that J_{4a} and J_{4b} have different signs: J_{4b} favors ordering and J_{4a} favors clustering. Accordingly, in the ordered $I4_122$ compound the 4b and 4a neighbors are occupied by dissimilar and similar pairs of cations, respectively (Fig. 1). Assigning the same negative ordering energy to all pairs of the fourth neighbors, as was done in the earlier studies, destabilized the ordered phase.

THERMODYNAMIC INTEGRATION

It has been shown (Myers et al. 1998; Myers 1999; Dove 2001) that the free energy of mixing can be calculated from Monte Carlo averaged excess energies using the method of λ-integration:

$$F = F_0 + \int_0^{\lambda} \langle E \rangle_{\lambda} d\lambda \quad (6)$$

In this equation F_0 corresponds to the free energy of mixing of the solid solution with zero ordering energy, which can be calculated exactly with:

$$F_0 = RT(x_{Mg} \ln x_{Mg} + x_{Ca} \ln x_{Ca}) \quad (7)$$

The integral describes the contribution to the free energy from the excess energy, when its value changes from the state of the complete disorder, $\langle E \rangle_{\lambda=0}$, to the equilibrium state of the order at

a given temperature. To simulate energy states with intermediate states of order one performs additional Monte Carlo simulations with scaled values of the J values:

$$J_n^{\lambda} = \lambda J_n \tag{8}$$

where λ varies between 0 and 1. Effectively, the scaling means that the probabilities of microstates become more random than in the non-scaled case. The $\langle E \rangle_{\lambda}$ is calculated by averaging the energies of the Monte Carlo states using Equation 2 with nominal (not scaled) values of J values. In our simulations, λ was gradually increased from 0 to 1 with a step of 0.025. The integral was calculated using Simpson's method. Figure 13a shows the free energy of mixing calculated from Monte Carlo results obtained with the T-I J values. These free energies of mixing ignore the effect of the excess vibrational free energy and the excess volume. However, at equilibrium the microstates with high excess vibrational entropy will occur more frequently than the low entropy states, particularly so at high temperatures. Thus the excess vibrational entropy has an effect on the configurational entropy. This effect is taken into account, when the thermodynamic integration analysis is applied to Monte Carlo averaged excess Gibbs free energies $\langle \phi \rangle_{\lambda}$. The averaged excess Gibbs energies should simply substitute the averaged excess enthalpies in Equation 6. Figure 13b shows the results of the thermodynamic integration analysis of the Monte Carlo results obtained with the temperature dependent J values, which correspond to 0 GPa. The isotherms in Figure13b include the effects of the configurational entropy and the excess vibrational free energy. The pure excess vibrational free energy is plotted in Figure 14. This function was calculated by subtracting the free energy of mixing obtained from the simulations with T-D J values, from the free energy of mixing obtained from the simulations with the T-I J values. The excess vibrational entropy can be approximately calculated from Figure 14 dividing the excess energies by $-T$.

The configurational entropy was calculated with the equation.

$$S = (F - \langle \phi \rangle)/T \tag{9}$$

where F is the total Gibbs free energy of mixing obtained using Equation 6 and $\langle \phi \rangle$ is the Monte Carlo averaged excess Gibbs free energy at zero pressure. Figure 15 shows the configurational entropy in the interval of 300–1500 K. A very similar result is obtained by applying the thermodynamic integration analysis to the averaged excess Gibbs free energies calculated at 3 GPa. The configurational entropy reflects the effects of SRO and LRO.

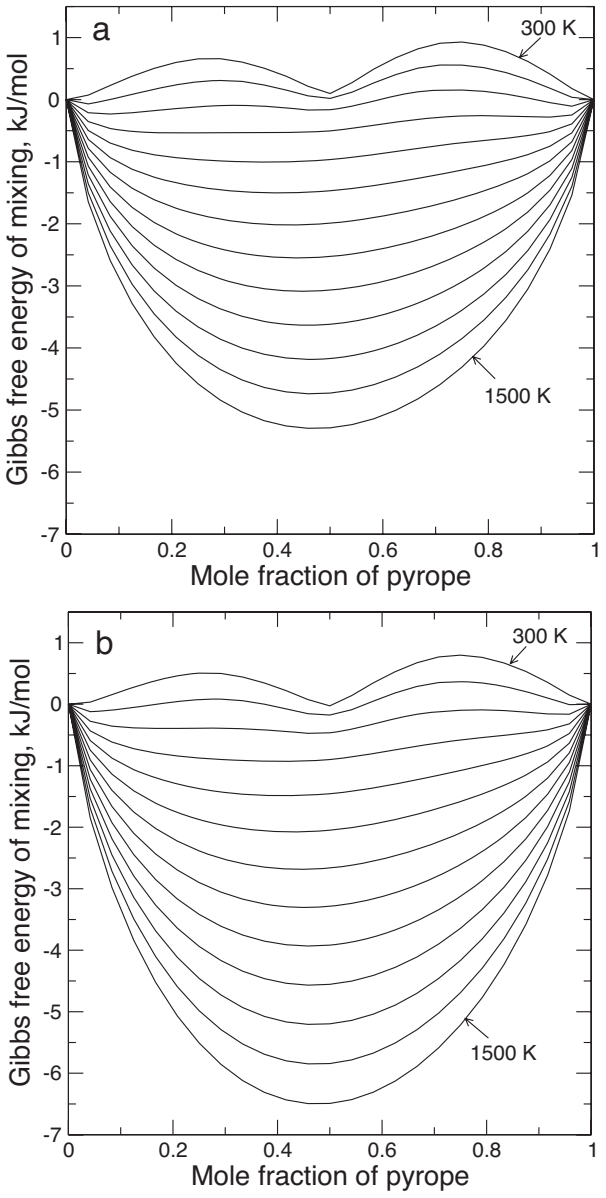

FIGURE 13. Gibbs free energy of mixing derived from the thermodynamic integration analysis of the Monte Carlo results. The cases **a** and **b** correspond to the simulations with the temperature-independent J values and temperature-dependent J values, respectively.

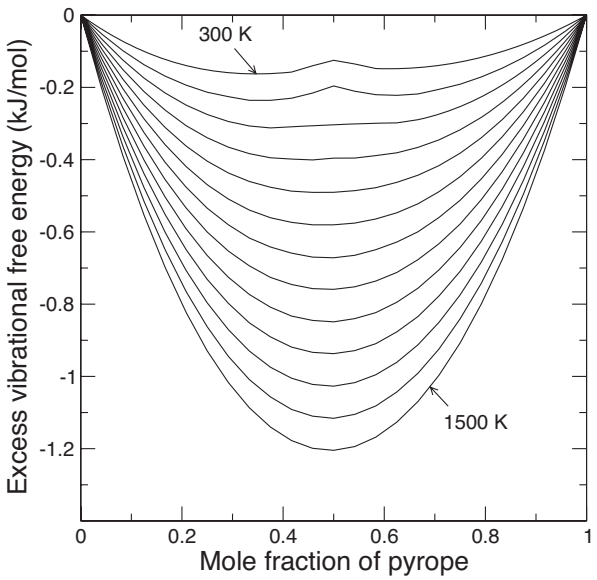

FIGURE 14. The excess vibrational free energy calculated as the difference between the free energies calculated with the temperature-dependent and temperature-independent J values.

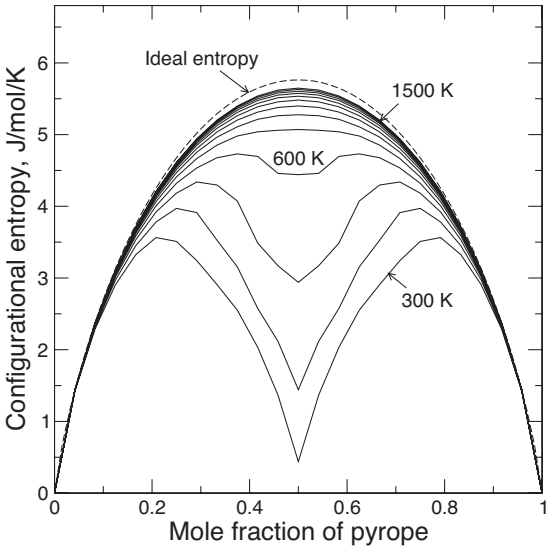

FIGURE 15. The configurational entropy calculated using the method of thermodynamic integration. Simulations were performed with the temperature dependent J values at zero pressure. The dashed line shows the entropy of ideal mixing.

The development of LRO is manifested by the rapid decrease in the entropy. The excess free energies of mixing behave more smoothly, but also reveal the effects of the ordering. The analysis of the curvature of the free energies of mixing, combined with the calculations of the onset of the LRO (Fig. 12), permits the drawing of the *T-X* phase diagrams. Practically, we tested if the free energy at each point along the isotherm is lower than the weighted sum of the free energies of any other two points of the isotherm. If this test is not fulfilled, the point is marked as "unstable." The miscibility gaps are shown as smoothed curves, which encircle the clusters of the unstable points. The phase diagrams shown in Figures 16a and 16b correspond to the free energies that ignore and include the vibrational free energies, respectively. Evidently, including vibrational effects stabilizes the intermediate phase. Figure 16c corresponds to the free energy of mixing calculated by the thermodynamic integration analysis applied to the excess Gibbs free energies corresponding to 3 Gpa. It appears that the intermediate compound is destabilized with pressure due to the increase in the PV_{ex} term.

Polynomial fit to the free energies of mixing

In many petrological models the free energy of mixing is separated into ideal and excess contributions. The excess free

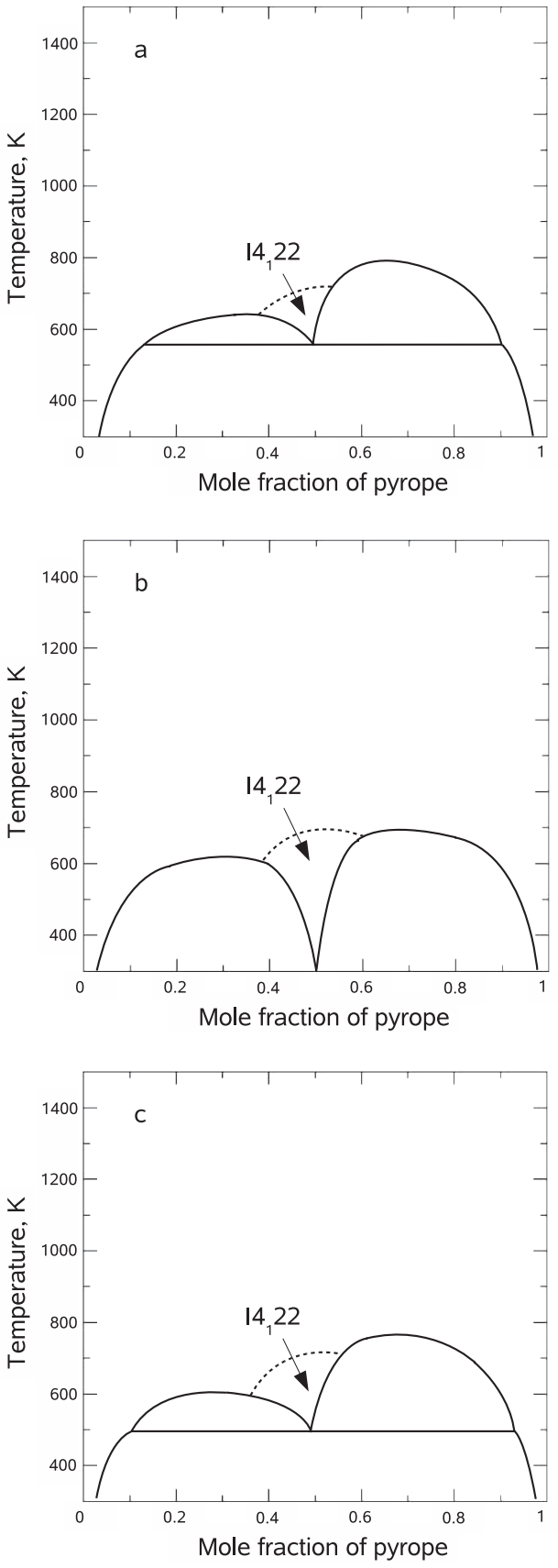

FIGURE 16. The temperature-composition phase diagrams calculated based on the results of Monte Carlo simulations. The cases (**a**) and (**b**) correspond to the simulations with the temperature-independent and temperature-dependent J values, respectively, performed at zero pressure. The difference in the topology is due to the effect of the excess vibrational free energy, which is included in the case **b**. Case **c** corresponds to the simulations with the temperature dependent J values calculated at 3 GPa. The difference in the topology relative to the case **b** is due to the PV_{ex} term.

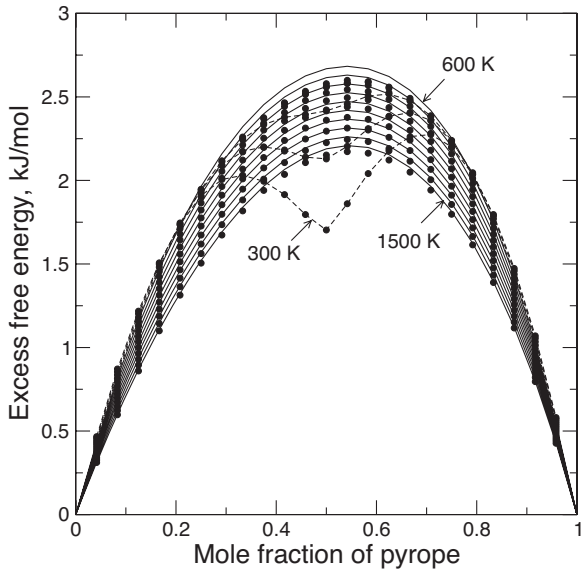

FIGURE 17. The excess free energy of mixing calculated by subtracting TS_{id} term from the total free energy of mixing. (The Monte Carlo calculations were performed with the temperature-dependent J values at zero pressure.) The solid dots are the Monte Carlo results and the solid lines are the results of the fit with the Redlich-Kister polynomial of the 5th order.

energies of mixing calculated by subtracting the $-TS_{ideal}$ term from the Monte Carlo free energies are plotted in Figure 17. At temperatures above 600 K, the excess free energies behave smoothly, thereby providing a possibility for a polynomial description. Table 7 lists the coefficients of the Redlich-Kister polynomial (Redlich and Kister 1948, see also Ganguly 2001) of the 5th order, which gives a reasonably accurate fit to the excess free energy in the range of 600–1500 K both at 0 and 3 GPa

$$G_{excess} = x_1 x_2 \sum_{n=1}^{6} (A_n - TB_n)(x_2 - x_1)^{n-1} \quad (10)$$

The excess free energy in the range of 300–600 K is very much perturbed due to the LRO effect. Figure 17 shows that the LRO causes the rapid decrease of the isotherms, which is most pronounced at 0.5. The part of the excess free energy, which is not described with the Redlich-Kister polynomial, can be fitted separately using the Gaussian

$$G_{ord} = x_1 x_2 (C_1 - TD_1 - T \ln TF_1) \exp(C_2 - TD_2)(x_1 - 0.5)^2 \quad (11)$$

where x_1 and x_2 are mole fractions of grossular and pyrope, respectively. The shape of the Gaussian function is particularly well suited to describe the dip in the free energy associated with the development of LRO. The coefficients of this function are listed in Table 8. For simplicity, we assume this function to be pressure independent. Equations 10 and 11 together permits an accurate fit to the excess free energies of mixing in the range of 300–1500 K at 0 GPa or at 3 GPa. Figure 18 plots the activities at 0 GPa, which are easily calculated from the excess free energies of mixing (e.g., Hillert 1998). The activity-composition relations corresponding to pressures in the range of 0–3 GPa can be calculated by linearly interpolating the Redlich-Kister coefficients

TABLE 7. Coefficients of the Redlich-Kister polynomial for the excess free energy in the grossular-pyrope solid solution

N	A_n (J/mol) 0 GPa	B_n (J/mol·K) 0 GPa	A_n (J/mol) 3 GPa	B_n (J/mol·K) 3 GPa
1	11953.7	2.1318	12656.2	1.6605
2	1237.4	−0.2627	1363.8	−0.2131
3	3783.6	2.1771	4100.1	2.3268
4	1505.3	1.2199	1321.8	1.1152
5	−1350.9	−0.9663	−1582.3	−1.0913
6	−1449.2	−1.1684	−1406.4	−1.1898

TABLE 8. Coefficients of the Gaussian for the description of the LRO effect on the excess free energy of mixing

N	C_n (J/mol)	D_n (J/mol·K)	F_n (J/mol/K/lnK)
1	−15145.7	−145.9	19.0
2	−22493.3	−17.3	

TABLE 9. Coefficients of the subregular model for the excess free energy in the grossular-pyrope solid solution [values are in J/mol, J/(K·mol), and J/(bar·mol) of exchangeable atoms]

Source	W^H_{CaMg}	W^H_{MgCa}	W^S_{CaMg}	W^S_{MgCa}	W^V_{CaMg}	W^V_{MgCa}
Ganguly et al. (1996)	21627	9834	5.780	5.780	0.012	0.058
Mukhopadhyay et al. (1997)	21721	4769	6.940	0.830	0.017	0.047
Berman and Aranovich (1996)	22760	11157	6.263	6.263	0.012	0.058
This study	13468	10038	1.948	1.704	0.043	0.041

(Table 8) corresponding to 0 and 3 GPa, respectively.

We have also performed the fit with the Redlich-Kister polynomial of the first order. This polynomial corresponds to a regular solid solution model with temperature- and pressure-dependent Margules parameters. Although the quality of this fit is low, it allows us to compare the present results with models constrained with phase equilibrium data. Table 9 lists our results together with the results of the three models, which are widely used in petrological calculations.

DISCUSSION

Our model of mixing differs from previously reported models of pyrope-grossular garnets in several aspects. First of all, it is an atomistic model, which includes the effects of ordering and lattice vibrations and predicts their magnitudes as functions of the temperature. It permits consistent explanation of the origin of the asymmetry of the mixing functions. The advanced feature of the model is the inclusion of quasi-harmonic lattice dynamics instead of relying exclusively on static lattice energy calculations. Previous simulation studies, with the exception of the recent work of Lavrentiev et al. (2006), are based on the SLEC only. Treating thermal expansion has also permitted us to reproduce the correct magnitude of the excess vibrational entropy. The average excess entropy at the intermediate composition is about 0.8 J/(mol·K) at 300 K and 1.1 J/(mol·K) at 1000 K (Figs. 5a and 5b), which is close to the value (1.17 J/mol/K) calculated by Lavrentiev et al. (2006) for a single configuration of $x_{pyr} = 0.5$ using a similar free energy minimization technique. Our estimates are of the same order of magnitude as that (1.5 J/mol/K) measured by Haselton and Westrum (1980) for their sample with $x_{pyr} = 0.6$. This is the main improvement over the study of Vinograd et al. (2004b), where much smaller excess entropies have been predicted. The other important feature of the model is the use of well-constrained interatomic potentials. Before starting the large-scale Monte Carlo simulations we have demonstrated a

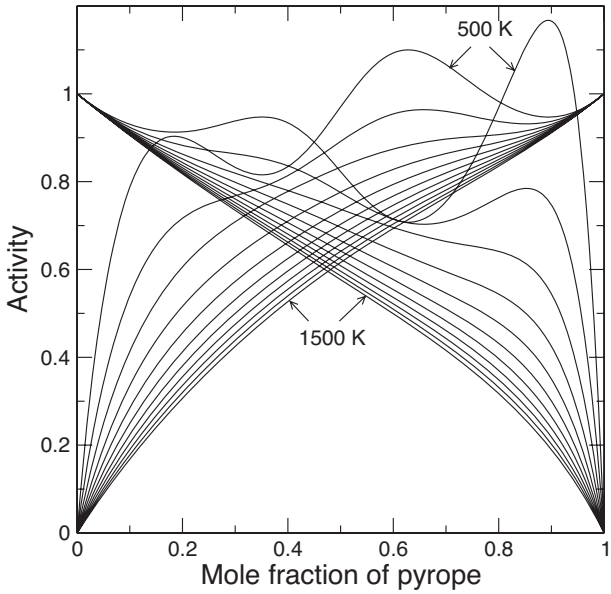

FIGURE 18. The activity-composition relations in the range of 500–1500 K at zero pressure in pyrope-grossular garnets calculated using the Redlich-Kister polynomial of the 5th order and the Gaussian function for the energy of ordering.

nearly perfect correspondence between the empirically based and ab initio calculated excess energies of a set of structures with different Ca/Mg ratios and different ordering states. This determines the near quantitative agreement of the present model with the calorimetric data of Newton et al. (1977). The previous simulation studies of Bosenick et al. (2001) and Lavrentiev et al. (2006) predicted significantly larger excess enthalpies. The excess volumes (Figs. 4a and 4b) have the same magnitude and the same type of asymmetry as the experimental data of Bosenick and Geiger (1997). However, the calculated properties cannot be directly compared to the experimental ones. The volume measurements of Bosenick and Geiger (1997) were done between 20 and 300 K, while the samples have been prepared by high temperature synthesis. Our calculations at 1000 K are more consistent with the measured volumes. It is possible that the measured volumes reflected the asymmetry quenched at the temperature of the synthesis. Here we assume that the quenched excess volume is determined by the atomic configurations, which have been in equilibrium at the temperature of the synthesis. At the synthesis temperature the configurations with large (and asymmetric) volumes and entropies would be favored. Presumably, the effect of the lattice contraction due to the decrease of the temperature is nearly the same for all the configurations and thus the asymmetry of the excess property can be quenched. A similar difficulty prevents the direct comparison of the measured and calculated excess vibrational entropies. The measurements of Haselton and Westrum (1980) have been performed in the range of 10–350 K, while the sample has been synthesized at 1623 K. The direct comparison would require a calculation of excess heat capacities and excess entropies in the range of 10–350 K for a large set of configurations, followed by configurational averaging at the temperature of the synthesis and application of Boltzmann weights to the results obtained for the low-temperature excess heat capacities or the excess entropies of the sampled configurations. We did not perform these calculations because we could not construct an accurate cluster expansion separately for the vibrational entropy. Using the free energy minimization for 125 different cation arrangements in the garnet unit cell we could show only that the excess volumes and the excess entropies substantially increase with the temperature (Figs. 4a, 4b, 5a, and 5b). The autocorrelation between the excess volumes and the entropies suggests that at the temperature of the synthesis the configurations, which have larger excess volumes and larger excess entropies, will be sampled with higher probabilities. It is thus possible that the excess entropy measured by Haselton and Westrum (1980) samples the atomic configurations, which have relatively high excess vibrational entropies. The entropies of these configurations remain relatively high even at the low temperatures at which the calorimetric measurements are made. The decrease of the excess entropy with the decrease in the temperature, observed in our calculations, suggests that real excess vibrational entropies, which affect garnet phase equilibria might be slightly lower than those which could be inferred from the result of Haselton and Westrum (1980). Therefore, our excess values plotted in Figure 5a are probably not significantly lower than the real ones. The results obtained from the configurational averaging of the excess free energies and from the regular model fit to the averaged free energies of mixing show that both the excess enthalpic and entropic Margules terms are lower than those suggested by models fitted to phase-equilibrium data (Table 9). These terms include both the vibrational and configurational effects. Our smaller value of the excess entropy term not only reflects the smaller excess vibrational entropy, but also the negative excess configurational entropy—the effect of the short-range order. The consistently lower magnitudes of the enthalpic and entropic terms (Table 9) do not imply that the predicted mixing properties differ significantly from those derived from phase equilibrium data. The effects of the excess enthalpy and entropy balance each other due to the relation $\Delta G = \Delta H - T\Delta S$. Therefore, models with very different Margules parameters could have nearly the same free energies of mixing. From the values of the excess terms given in Table 9 one can deduce that the excess free energy of our model will be nearly equal to that of the model of Berman and Aranovich (1996) at about 800–900 °C, i.e., at the typical conditions of phase equilibrium experiments. Therefore, our model is consistent with phase equilibrium data at least in this temperature interval.

The main difficulty of the present model is its inconsistency with the recent experimental results of Dachs and Geiger (2006) on the low-temperature excess heat capacity in the pyrope-grossular solid solution. In fact, the results of Dachs and Geiger (2006) show that the maximum of the excess vibrational entropy at 300 K occurs at pyrope-rich compositions, in contradiction to our prediction. It follows then that our speculations on the origin of the excess entropy and its asymmetry based on the virtual crystal model could be wrong. The other possibility is that the inconsistency arises due to large experimental errors inherent in the method of the heat pulse calorimetry (HPC) used in the study of Dachs and Geiger (2006). Dachs and Geiger (2006) admit that the HPC, despite its many advantages (e.g., a smaller sample size), still has a lower accuracy than adiabatic calorimetry.

Dachs and Geiger (2006) were able to reproduce the result of Haselton and Westrum (1980) for the excess heat capacity of Pyr60 (the same sample was used in both studies) only in the low-temperature (5–40 K) interval. The measurements at higher temperatures predicted negative heat capacities that have resulted in significantly lower total excess entropy at 300 K. The S_{300} value of Dachs and Geiger (2006) amounts to about 0.35 of the value of Haselton and Westrum (1980). Dachs and Geiger (2006) in their Figures 4a and 4b show that the errors in the calculated heat capacities become increasingly large at high-temperatures. This observation suggests that the HPC results are reliable only at relatively low temperatures. The excess heat capacities collected by Dachs and Geiger (2006) in the interval of 5–30 K show the pronounced asymmetry with the maximum at grossular-rich compositions in good agreement with our results.

It is clear, however, that new measurements are needed to resolve the contradiction between the results of Haselton and Westrum (1980) and Dachs and Geiger (2006). The results of the HPC and the adiabatic calorimetry should be compared for samples with different compositions. It is also necessary to test the predictions of the present study related to the asymmetry of the mixing functions on different systems with comparable size mismatch between the exchangeable cations.

Our study has permitted not only to simulate the excess mixing, but also to understand the driving forces of cation ordering. We have observed that the magnitudes of the ordering interactions, the *J* values, can be explained on structural grounds. This has become particularly obvious, when we have distinguished the local pair-wise ordering constants not merely based on the distances, but based more correctly on the symmetry of the pairs. We have shown that the pairs 4a and 4b, despite their equal length (Fig. 1b), reveal contrasting ordering behavior. Apparently, the much stronger ordering tendency along the 4b pair is related to the presence of Al atom exactly in the middle of the two dodecahedral cations: The rigid AlO_6 polyhedron restricts significantly the space available for the bond-distance relaxation and, therefore, at the intermediate composition the two differently sized dodecahedral cations have a stronger tendency to alternate. Although similar arguments have been used already to explain the very strong ordering tendency at the third near-neighbor distance (Bosenick et al. 2000; Vinograd et al. 2004a), it is now clear that this is a widely occurring phenomenon. The strong interactions are related to the presence of extra cations such as Si (in the case of J_3) or Al (in the case of J_{4b}). Interestingly, the cluster expansion analysis of the Ca-Mg interactions in carbonates (Vinograd et al. 2006b) shows that the strongest ordering interaction occurs there at the fourth near-neighbor distance. The fourth neighbors interact across the rigid CO_3 group.

The arguments given above do not explain, however, the relatively strong interaction along the 5th near-neighbor pair and the absence of significant ordering at the first and second distances. Apparently, there are other factors influencing the strength of local ordering. The absence of strong ordering within the first neighbors can be related to the frustration phenomenon. The first neighbors make a frame of triangular clusters. Perfect alternation is impossible within such a framework and this is consistent with the near zero value of J_1. The same argument is probably valid for J_2 interactions. The second neighbors form frustrated triangular clusters together with the first neighbors. The strong interaction at the 5th distance can be attributed to the fact that J_3 and J_{4b} interactions together with J_5 form a non-frustrated three-dimensional framework, which can be perfectly ordered. In fact, the ordered $I4_122$ structure implies the maximum number of dissimilar, Ca-Mg, pairs at these three distances. The large negative value of J_5 might simply reflect the general tendency to $I4_122$ ordering, which is driven by J_3 and J_{4b}.

The ability to distinguish 4a and 4b interactions has allowed us to predict that the $I4_122$ structure is the most stable intermediate compound. Our SLEC and ab initio calculations both show that the excess energy of this structure is only slightly above the energy of a mixture of equal amounts of pyrope and grossular. The Monte Carlo analysis suggests that this structure, not being the ground state, becomes stable in a certain temperature interval due to the excess negative vibrational free energy. This shows that the analysis of vibrations could be very important for determining the topology of phase diagrams of silicate systems with size mismatch. The predicted phase diagram with two nearly symmetric miscibility gaps offers a different explanation to the immiscibility in pyrope- and grossular-rich garnet described by Wang et al. (2000). The unmixing could have occurred due to a low-temperature dissolution/reprecipitation process triggered by a fluid phase. The near equality of the energy of the 50/50 compound to the equal mixture of the end-members is probably a common phenomenon in solid solutions with size-mismatch. The ordering energy arises due to the relaxation of the elastic energy of the strained mixture of the end-members, which becomes possible due to the formation of pairs of cations of dissimilar size. In the 50/50 compound the proportion of the strained AA- and BB-type pairs can be minimized due to the formation of the less strained AB-type pairs. In the case of the garnet structure not all AA and BB pairs can be avoided because of the frustration. However, the avoidance of the most unfavorable 3rd, 4th, and 5th AA and BB pairs becomes possible in the $I4_122$ structure. This explains the nearly zero excess energy of this compound.

The present analysis of the origin of the effects of mixing and ordering in pyrope-grossular garnets suggests that the total enthalpy of mixing is caused by the global strain, which is caused by the size mismatch between Ca and Mg and that is accumulated within CaCa and MgMg pairs. This strain is locally released via the formation of CaMg pairs. This conclusion is in accord with the results of the recent synchrotron X-ray powder diffraction study of Dapiaggi et al. (2005), which suggested that the enthalpy of mixing in pyrope-grossular garnets may be related to the microscopic strain measured as a function of the average fluctuations in the interplanar distances about their ideal values. According to our model, the residual strain is accumulated within MgMg and CaCa pairs, which are too short or too long, respectively, to fit the ideal interatomic distances at intermediate compositions. Assuming that the mean *d*-spacing fluctuation correlates with the number of MgMg and CaCa pairs at the distance *d* (these pairs should deviate stronger than CaMg pairs from the ideal spacing), the same correlation should exist between the *d*-spacing fluctuation and the enthalpy of mixing. This speculation supports the current belief that the peak-broadening correlates with the excess enthalpy. It is also conceivable that mixing effects in the other binaries of $(Ca,Mg,Fe,Mn)_3Al_2Si_3O_{12}$ garnets should

scale with the size difference of the cations. This correlation has been already described in the reviews by Geiger (1999, 2001).

ACKNOWLEDGMENTS

The authors thank Björn Winkler and Julian D. Gale for assistance with calculations and for discussions. The comments from Charles Geiger, John Purton, and two anonymous reviewers were very helpful also. The support of the Deutsche Forschungsgemeinschaft (grant Wi 1232/14-2) is gratefully acknowledged. MS gratefully acknowledges support of the Stichting voor Fundamenteel Onderzoek der Materie (Foundation for Fundamental Research of Matter), through financial support from the Nederlandse Organisatie voor Wetenschappelijk Onderzoek NWO (Netherlands Organization for Scientific Research).

REFERENCES CITED

Allan, N.L., Barron, T.H.K., and Bruno, J.A.O. (1996) The zero static internal stress approximation in lattice dynamics, and the calculation of isotope effects on molar volumes. Journal of Chemical Physics, 105, 8300–8303.

Angel, R.J., Carpenter, M.A., and Finger, L.W. (1990) Structural variation associated with compositional variation and order-disorder behavior in anorthite-rich feldspars American Mineralogist, 75, 150–162.

Bass, J.D. (1989) Elasticity of grossular and spessartine garnets by Brillouin spectroscopy. Journal of Geophysical Research, 84, 7621–7628.

——— (1995) Elasticity of minerals, glasses, and melts. In Th. Ahrens, Ed., Mineral Physics and Crystallography. A Handbook of Physical Constants. AGU Reference Shelf 2. 45 p. American Geophysical Union, Washington, D.C.

Berman, R.G. and Aranovich, L.Y. (1996) Optimized standard state and solution properties of minerals. I. Model calibration for olivine, orthopyroxene, cordierite, garnet, and ilmenite in the system FeO-MgO-CaO-Al_2O_3-TiO_2-SiO_2. Contributions to Mineralogy and Petrology, 126, 1–24.

Boffa Ballaran, T., Carpenter, M.A., Geiger, C.A., Koziol, A.M. (1999) Local structural heterogeneity in garnet solid solutions. Physics and Chemistry of Minerals, 26, 554–569.

Bosenick, A. and Geiger, C.A. (1997) Powder X-ray diffraction study of synthetic pyrope-grossular garnets between 20 and 295 K: A comparison of thermal expansion and heat capacity and volumes of mixing. Journal of Geophysical Research, 102, 22649–22657.

Bosenick, A., Geiger, C.A., Schaller, T., and Sebald, A. (1995) A ^{29}Si MAS NMR and IR spectroscopic investigation of synthetic pyrope-grossular garnet solid solutions. American Mineralogist, 80, 691–704.

Bosenick, A., Geiger, C.A., and Cemic, L. (1996) Heat capacity measurements of synthetic pyrope-grossular garnets between 320 and 1000 K by differential scanning calorimetry. Geochimica et Cosmochimica Acta, 60, 3215–3227.

Bosenick, A., Geiger, C.A., and Phillips, B.L. (1999) Local Ca-Mg distribution of Mg-rich pyrope-grossular garnets synthesized at different temperatures revealed by ^{29}Si MAS NMR spectroscopy. American Mineralogist, 84, 1422–1432.

Bosenick, A., Dove, M.T., and Geiger, C.A. (2000) Simulation studies of pyrope-grossular solid solutions. Physics and Chemistry of Minerals, 27, 398–418.

Bosenick, A., Dove, M.T., Heine, V., and Geiger, C.A. (2001a) Scaling of thermodynamic mixing properties in garnet solid solutions. Physics and Chemistry of Minerals, 28, 177–187.

Bosenick, A., Dove, M.T., Myers, E.R., Palin, E.J., Sainz-Diaz, C.I., Guiton, B.S., Warren, M.C., and Craig, M.S. (2001b) Computational methods for the study of energies of cation distributions: applications to cation-ordering phase transitions and solid solutions. Mineralogical Magazine, 65, 193–219.

Dachs, E. and Geiger, C.A. (2006) Heat capacities and entropies of mixing of pyrope-grossular ($Mg_3Al_2Si_3O_{12}$-$Ca_3Al_2Si_3O_{12}$) garnet solid solutions: A low-temperature calorimetric and a thermodynamic investigation. American Mineralogist, 91, 894–906.

Dapiaggi, M., Geiger, C.A., Artioly, G. (2005) Microscopic strain in synthetic pyrope-grossular solid solutions determined by synchrotron X-ray powder diffraction at 5 K: The relationship to enthalpy of mixing behavior. American Mineralogist 90, 506–509.

Dove, M.T. (2001) Computer simulations of solid solutions. In Ch. Geiger, Ed., Solid Solutions in Silicate and Oxide Systems of Geological Importance. EMU Notes in Mineralogy, 3, 225–250. Eötvös University Press, Budapest.

Ferreira, L.G., Mbaye, A.A., and Zunger, A. (1988) Chemical and elastic effects on isostructural phase diagrams: The e-G approach. Physical Review B, 37, 10547–10570.

Gale, J.D. (1996) Empirical derivation of interatomic potentials for ionic materials. Philosophical Magazine B, 73, 3–19.

——— (1997) GULP—a computer program for the symmetry adapted simulation of solids. Journal of Chemical Society: Faraday Transactions, 93, 629–637.

Ganguly, J. (2001) Thermodynamic modeling of solid solutions. In C. Geiger, Ed., Solid Solutions in Silicate and Oxide Systems of Geological Importance. EMU Notes in Mineralogy, 3, 37 p. Eötvös University Press, Budapest.

Ganguly, J., Cheng, W., and O'Neil, H.St.C. (1993) Syntheses, volume, and structural changes of garnets in the pyrope-grossular join: Implications for stability and mixing properties. American Mineralogist, 78, 583–593.

Ganguly, J., Cheng, W., and Tirone, M. (1996) Thermodynamics of aluminosilicate garnet solid solution: new experimental data, an optimized model, and thermometric applications. Contributions to Mineralogy and Petrology, 126, 137–151.

Geiger, C.A. (1999) Thermodynamics of $(Fe^{2+},Mg^{2+},Mn,Ca)_3Al_2Si_3O_{12}$ garnet: a review and analysis. Mineralogy and Petrology, 66, 271–299.

——— (2001) Thermodynamic mixing properties of binary oxide and silicate solid solutions determined by direct measurements: The role of strain. In C. Geiger, Ed., Solid Solutions in Silicate and Oxide Systems of Geological Importance. EMU Notes in Mineralogy, 3, 71 p, Eötvös University Press, Budapest.

Geiger, C.A. and Armbruster, T. (1997) $Mn_3Al_2Si_3O_{12}$ spessartine and $Ca_3Al_2Si_3O_{12}$ grossular garnet: Structural dynamics and thermodynamic properties. American Mineralogist, 82, 740–747.

Haselton, H.T. Jr. and Westrum, E.F. Jr. (1980) Low-temperature heat capacities of synthetic pyrope, grossular, and $pyrope_{60}grossular_{40}$. Geochimica et Cosmochimica Acta, 44, 701–709.

Hillert, M. (1998) Phase equilibria, phase diagrams and phase transformations: Their thermodynamic basis. Cambridge University Press, Cambridge, U.K.

Hohenberg, P. and Kohn, W. (1964) Inhomogeneous electron gas. Physical Review 136, B864–B871.

Isaak, D.G., Anderson, O.L., and Oda, H. (1992) High-temperature thermal expansion and elasticity of calcium-rich garnets. Physics and Chemistry of Minerals, 19, 106–120.

Jones, R.O. and Gunnarsson, O. (1989) The density functional formalism, its applications and prospects. Reviews in Modern Physics, 61, 689–746.

Kohn, W. and Sham, L.J. (1965) Self-consistent equations including exchange and correlation effects. Physical Review, 140, A1133–A1138.

Kolesov, B.A. and Geiger, C.A. (1998) Raman spectra of silicate garnets. Physics and Chemistry of Minerals, 25, 142–151.

Kresse, G. and Furthmüller, J. (1996) Efficient iterative schemes for ab initio total energy calculations using a plane wave basis set. Physical Review, B54, 11169–11186.

Kresse, G. and Hafner, J. (1994) Norm-conserving and ultrasoft pseudopotentials for first-row and transition elements. Journal of Physics: Condensed Matter 6, 8245–8257.

Lavrentiev, M.Yu., van Westrenen, W., Allan, N.L., Freeman, C.L., and Purton, J.A. (2005) Simulation of thermodynamic mixing properties of garnet solid solutions at high temperatures and pressures. Chemical Geology, 225, 336–346.

Leitner, B.J., Weidner, D.J., and Liebermann, R.C. (1980) Elasticity of single crystal pyrope and implications for garnet solid solution series. Physics of Earth and Planetary Interiors, 22, 111–121.

Metropolis, N.I., Rosenbluth, A.W., Rosenbluth, M.N., Teller, A.N. and Teller, E. (1953) Equation of state calculations by fast computing machines. Journal of Chemical Physics 21, 1087–1092.

Myers, E.R. (1999) Al/Si ordering in silicate minerals, Ph.D. thesis. University of Cambridge, U.K.

Myers, E.R., Heine, V., and Dove, M.T. (1998) Some consequences of Al/Al avoidance in the ordering of Al/Si tetrahedral framework structures. Physics and Chemistry of Minerals, 25, 457–464.

Mukhopadhyay, B., Holdaway, M.J., and Koziol, A.M. (1997) A statistical model of the thermodynamic mixing properties of Ca-Mg-Fe^{2+} garnets. American Mineralogist, 82, 165–181.

Newton, R.C., Charlu, T.V., and Kleppa, O.J. (1977) Thermochemistry of high pressure garnets and clinopyroxenes in the system CaO-MgO-Al_2O_3-SiO_2. Geochimica et Cosmochimica Acta, 41, 369–377.

O'Neill, B., Bass, J.D., Rossman, G.R., Geiger, C.A., and Langer, K. (1991) Elastic properties of pyrope. Physics and Chemistry of Minerals, 17, 617–621.

Parr, R.G. and Yang, W. (1989) Density-functional theory of atoms and molecules. 342 p. Oxford University Press, New York.

Patel, A., Price, G.D., and Mendelsson. M.J. (1991) A computer-simulation approach to modeling the structure, thermodynamics and oxygen isotope equilibria of silicates. Physics and Chemistry of Minerals, 17, 690–699.

Pavese, A., Artioli, G., and Prencipe, M. (1995) X-ray single-crystal diffraction study of pyrope in the temperature range 30–973 K. American Mineralogist, 80, 457–464.

Perdew, J.P., Burke, K., and Ernzerhof, M. (1996) Generalized gradient approximation made simple. Physical Review Letters, 77, 3865–3868.

Redlich, O. and Kister, A.T. (1948) Thermodynamics of non-electrolyte solutions, x-y-t relations in a binary system. Industrial and Engineering Chemistry, 40, 341–345.

Rodehorst, U., Geiger, C.A., and Armbruster, T. (2002) The crystal structures of grossular and spessartine between 100 and 600 K and the crystal chemistry of grossular-spessartine solid solutions. American Mineralogist, 87, 542–549.

Sainz-Diaz, C.I., Hernandez-Laguna, A., and Dove, M.T. (2001) Modeling of dioctahedral 2:1 phyllosilicates by means of transferable empirical potentials. Physics and Chemistry of Minerals, 28, 130–141.

Sanders, M.J., Leslie, M., and Catlow, C.R. (1984) Interatomic potentials for SiO_2. Journal of the Chemical Society, Chemical Communications, 19, 1271–1273.

Sluiter, M.H.F., Vinograd, V.L., and Kawazoe, Y. (2004) Intermixing tendencies in garnets: Pyrope and grossular. Physical Review B70, 184120–1,184120-4.

Swainson, I.P., Dove, M.T., Schmahl, W.W., Putnis, A. (1992) Neutron diffraction study of the akermanite-gehlenite solid solution series. Physics and Chemistry

of Minerals, 19, 185–195.
Vanderbilt, D. (1990) Soft self-consistent pseudopotentials in a generalized eigenvalue formalism. Physical Review B41, 7894–7895.
Vinograd, V.L. (2001) Configurational entropy of binary silicate solid solutions. In Ch. Geiger, Ed., Solid Solutions in Silicate and Oxide Systems of Geological Importance. EMU Notes in Mineralogy, 3. 303 p. Eötvös University Press, Budapest.
Vinograd, V.L. and Putnis, A. (1999) The description of Al,Si ordering in aluminosilicates using the cluster variation method. American Mineralogist, 84, 311–324.
Vinograd, V.L., Sluiter, M.H.F., Winkler, B., Putnis, A., and Gale, J.D. (2004a) Thermodynamics of mixing and ordering in silicates and oxides from static lattice energy and ab initio calculations. In M. Warren, A. Oganov and B. Winkler, Eds., First-Principles Simulations: Perspectives and Challenges in Mineral Sciences. Deutsche Gesellschaft für Kristallographie. Berichte aus Arbeitskreisen der DFK, 14, 143 p.
Vinograd, V.L., Sluiter, M.H.F., Winkler, B., Putnis, A., Hålenius U., Gale, J.D., and Becker, U. (2004b) Thermodynamics of mixing and ordering in the pyrope-grossular solid solution. Mineralogical Magazine, 68, 101–121.
Vinograd, V.L.,Winkler, B., Putnis, A., Kroll, H., Milman, V., Gale, J.D., and Fabrichnaya, O. B. (2006a) Thermodynamics of pyrope-majorite, $Mg_3Al_2Si_3O_{12}$-$Mg_4Si_4O_{12}$, solid solution from atomistic model calculations. Molecular Simulations, 32, 85–99.
Vinograd, V.L., Winkler, B., Putnis, A., Gale, J.D., and Sluiter, M.H.F. (2006b). Static lattice energy calculations of mixing and ordering enthalpy in binary carbonate solid solutions. Chemical Geology, 225, 304–313.
Wang, L., Essene, E.J., and Zhang, Y. (2000) Direct observation of immiscibily in pyrope-almandine-grossular garnet. American Mineralogist, 85, 41–46.
Warren, M.C., Dove, M.T., Myers, E.R., Bosenick, A., Palin, E.J., Sainz-Diaz, C.I., and Guiton, B.S. (2001) Monte Carlo methods for the study of cation ordering in minerals. Mineralogical Magazine, 65, 221–248.
Winkler, B., Dove, M.T., and Leslie, M. (1991) Static lattice energy minimization and lattice dynamics calculations on aluminosilicate minerals. American Mineralogist, 76, 313–331.
Zhang, L., Ahsbahs, H., and Kutoglu, A. (1998) Hydrostatic compression and crystal structure of pyrope to 33 GPa. Physics and Chemistry of Minerals, 25, 301–307.
Zhang, L., Ahsbahs, H., Kutoglu, A., and Geiger, C.A. (1999) Single-crystal hydrostatic compression of synthetic pyrope, almandune, spessartine, grossular and andradite at high pressures. Physics and Chemistry of Minerals, 27, 52–58.

MANUSCRIPT RECEIVED NOVEMBER 9, 2005
MANUSCRIPT ACCEPTED JUNE 14, 2006
MANUSCRIPT HANDLED BY KEVIN ROSSO